Published in final edited form as:
J Magn Reson Imaging. 2014 June ; 39(6): 1401–1410. doi:10.1002/jmri.24320.

Bone marrow uptake of ferumoxytol: a preliminary study in healthy human subjects

Pippa Storey, Ph.D. and **Arnaldo A. Arbini, M.D.**[2]

[1]Department of Radiology, New York University School of Medicine

[2]Department of Pathology, New York University School of Medicine

Abstract

Purpose—To characterize the uptake and elimination of ferumoxytol, an ultrasmall superparamagnetic iron oxide (USPIO) agent, in bone marrow of healthy human subjects.

Materials and methods—Four men and two postmenopausal women, aged 22 to 57 years, were prospectively included. Simultaneous fat, water and T_2^* mapping of the proximal femora was performed at 1.5 tesla using a 3D multiple gradient echo sequence. After baseline imaging, ferumoxytol (Feraheme/Rienso) was injected intravenously at a dose of 5 mg Fe/kg body weight. Imaging was repeated at 3 days, 1 month, 3 months and 5 months after administration.

Results—Imaging at 3 days revealed large increases in $R_2^*(=1/T_2^*)$ in hematopoietic marrow and lower average responses in fatty marrow, consistent with macrophage-specific uptake. However, certain regions of the diaphysis exhibited substantial R_2^* enhancement despite having high fat content. This suggests the persistence of residual marrow stroma following adipose conversion, and may reflect the ability of diaphyseal marrow to adapt dynamically to fluctuating demand for hematopoiesis. Follow-up imaging demonstrated almost complete R_2^* recovery within 3 months.

Conclusion—The observed R_2^* enhancement characteristics support applications for ferumoxytol in distinguishing normal or hypercellular marrow from neoplasms, infection and inflammation. Further studies are warranted in specific patient populations.

Keywords

MRI; USPIO; ferumoxytol; bone marrow; macrophage; iron

Introduction

Ultrasmall superparamagnetic iron oxide (USPIO) particles exhibit macrophage-specific uptake and dramatically shorten MRI relaxation times, making them potential candidates for imaging the mononuclear phagocyte system and for detecting disease processes involving macrophage infiltration. Their small size retards clearance by the liver and spleen and

---

Corresponding author: Pippa Storey, Center for Biomedical Imaging, Department of Radiology, New York University School of Medicine, 660 First Avenue New York, NY 10016, Tel: (212) 263-4854, Fax: (212) 263-7541, pippa.storey@nyumc.org.

facilitates migration across capillary walls (1), promoting uptake by resident or infiltrative macrophages in tissues such as bone marrow, lymph nodes and atherosclerotic plaque.

A promising application of USPIO particles in bone marrow is discrimination of tumor from hematopoietic marrow in cases where the marrow is highly cellular, due either to the young age of the patient or to therapy-induced reconversion. Hypercellular marrow and neoplastic tissue are difficult to distinguish using conventional marrow imaging protocols, which typically comprise T_1-weighted and fat-suppressed T_2-weighted fast spin-echo sequences (2–3). Gadolinium-based contrast agents provide little additional benefit, since both hypercellular marrow and neoplastic tissue demonstrate signal enhancement following gadolinium administration (3). USPIO particles, however, offer a means of discrimination since they are phagocytosed by resident macrophages in hematopoietic marrow but exhibit minimal uptake in tumor (2–6).

USPIO agents have likewise shown promise for improving the specificity of MRI for identifying osteomyelitis (7–8). The classic imaging features of osteomyelitis, namely edema and post-gadolinium signal enhancement, are also observed in the setting of inflammation, tumor, degenerative diseases and trauma (9). One distinguishing characteristic of osteomyelitis, however, is the presence of macrophage infiltration. In response to infection, a massive influx of phagocytes occurs, involving neutrophils and macrophages that replace normal bone marrow (8–9). The infiltrating macrophages take up USPIO particles, although not as avidly as normal hematopoietic marrow (9). This allows discrimination of osteomyelitis from neoplasms and sterile inflammation, which exhibit minimal uptake (7–8), and from healthy hematopoietic marrow, which shows greater uptake (7, 9).

In June 2009, ferumoxytol (Feraheme) became the first USPIO agent to be approved for human use in the United States. Prior to that date, the only superparamagnetic iron oxide (SPIO) agent available for intravenous administration in the U.S. was ferumoxides (Feridex/Endorem), which has relatively low uptake in bone marrow due to its large particle size (2). Ferumoxytol has also been approved in Canada and, more recently, in the European Union and Switzerland, where it is marketed under the brand name Rienso. It is indicated for the treatment of iron deficiency anemia in adult patients with chronic kidney disease, but can be used off-label as an MRI contrast agent. Experiments in rodents have shown that it produces persistent signal loss in hematopoietic marrow on T_2^*-weighted images (10).

The purpose of this preliminary study was to investigate changes in marrow $R_2^* (=1/T_2^*)$ following ferumoxytol injection in healthy human subjects. Quantification of R_2^* in marrow is complicated by the tissue's high fat content, which renders the signal decay non-exponential. Fat is present in both yellow and red marrow; yellow marrow consists primarily of adipocytes, while red marrow contains a mixture of adipocytes and hematopoietic elements in variable proportions (11). The lipid content, furthermore, provides valuable complementary information about marrow composition, since it differs between red and yellow marrow and among various pathological conditions. To maximize the accuracy of R_2^* measurements and enable simultaneous quantification of local fat content, complex-valued image data were acquired with a multiple-echo gradient echo sequence and analyzed using spectral fitting.

Materials and methods

Study Cohort

The study was performed under a protocol approved by the Institutional Review Board of our medical center. Among the exclusion criteria were pregnancy, a history of anaphylactic reaction, and iron overload as determined by baseline T_2^* imaging of the liver. A mean liver T_2^* shorter than 24 ms at 1.5 T was used as the criterion for elevated iron load (12). Six healthy subjects were included in the study (see Table 1) and all provided informed consent to participate. The group comprised four men and two post-menopausal women, aged 22 – 57 years, none of whom reported having anemia or any chronic disease.

Contrast Agent

Ferumoxytol (AMAG Pharmaceuticals, Cambridge, Massachusetts) is a colloidal solution of iron oxide nanoparticles formulated with mannitol. Each particle consists of a superparamagnetic magnetite core of about 6.8 nm in diameter covered with a semisynthetic carbohydrate coating of polyglucose sorbitol carboxymethylether, giving an overall particle size of 17 – 31 nm in solution. The coating isolates the bioactive iron from plasma components, allowing for safe bolus administration and resulting in a plasma half-life of about 16 hours in humans (13). When used for its approved indication as an iron replacement therapy, the recommended dose of ferumoxytol is two intravenous injections of 510 mg Fe each, administered at an interval of 3 – 8 days. In the present study, a dose of 5 mg Fe/kg body weight was used. Over our study cohort, this was equivalent to 318 – 501 mg of iron (see Table 1).

Study Protocol

Imaging was performed on a 1.5 T Avanto system (Siemens Healthcare, Erlangen, Germany), using body phased array coils in combination with spine coil elements in the patient table for signal reception. The first scan was performed before USPIO administration, and was used to screen for pre-existing iron overload and to collect baseline data. Ferumoxytol was injected as an intravenous bolus within 32 days of the initial scan, and imaging of bone marrow response was performed three days later. This interval was chosen since it corresponded to approximately five times the reported plasma half-life of the agent, and was therefore expected to coincide with peak macrophage uptake. To monitor subsequent iron elimination from the bone marrow, further scans were conducted at 1 month, 3 months and 5 months.

Image Acquisition

A multiple gradient echo (MGRE) sequence was used to perform simultaneous fat, water and T_2^* mapping of bone marrow in the proximal femora. A 3D slab was prescribed in an oblique coronal plane with a 400 × 400 mm^2 field of view (FOV) that extended from above the hips to just above the knees. For each line of *k*-space, 128 echoes were acquired using monopolar readout gradients, with a receiver bandwidth (BW) of 1000 Hz/pixel and an echo spacing of ΔTE = 1.83ms. This echo spacing was short enough to allow unambiguous identification of fat and water components, while the echo train was sufficiently long to permit calculation of a spectrum for each voxel. Spectra were generated by performing a Fourier transform of the complex-valued MGRE signal over the echo dimension. The minimum echo time TE_{min} was matched to the echo spacing (i.e. 1.83 ms) to eliminate the need for first order phase correction of the spectra. Ten partitions were acquired with a slice thickness of 2.1 mm and an in-plane matrix size of 192 × 192, providing isotropic 2.1 mm spatial resolution. A flip angle (FA) of 25° was used in combination with a repetition time (TR) of 255 ms, ensuring negligible T_1 weighting. The total acquisition time was 8 min 9 sec.

Calculation of fat, water and R_2^* maps

Image reconstruction was performed offline, retaining the phase as well as the magnitude of the signal for every echo in each voxel. Maps of fat, water and R_2^* were generated by performing a voxel-by-voxel fit of the complex-valued image data as a function of echo time. The model used for the fitting procedure assumed a single relaxation rate R_2^* for water and lipid components within the same voxel, and took into account the multiple spectral peaks of fat by using the signal from subcutaneous adipose tissue as a reference. The signal from each voxel within the imaging volume was assumed to be a linear combination of the reference fat signal plus a contribution from water, both attenuated by R_2^* dephasing due to the local environment. The model also incorporated an overall frequency offset to account for shimming imperfections and an overall phase offset representing the relative phase between the transmit and receive coils. The signal $S(t_n)$ as a function of time could thus be expressed as

$$S(t_n)=[W+Ff(t_n)]\exp(-R_2^* t_n)\exp[i(\varphi+\omega t_n)], \quad [1]$$

where $t_n = n.\Delta TE$ is the time of the n^{th} echo, W and F are the magnitudes of the water and fat components respectively, R_2^* is the local relaxation rate, and ϕ and ω are the local phase and frequency offsets respectively. The fitted parameters W, F, R_2^*, ϕ and ω are all real, while the functions $S(t_n)$ and $f(t_n)$ are both complex. $f(t_n)$ can be expanded as

$$f(t_n)=A_{\mathrm{norm}}S_{\mathrm{fat}}(t_n)\exp\left(R_2^{*(\mathrm{fat})}t_n\right), \quad [2]$$

and represents a normalized, R_2^*-corrected form of the reference fat signal $S_{fat}(t_n)$, which was measured in subcutaneous fat on the complex-valued MGRE images. To maximize its signal to noise ratio, $S_{fat}(t_n)$ was evaluated in a subject with high body mass index, and data from several adjacent voxels were combined. $R_2^{*(\mathrm{fat})}$ denotes the relaxation rate of the lipid components in the measured fat signal. It was estimated from the full width at half maximum (FWHM) of the principal (methylene) peak in the fat spectrum, which was generated by taking a Fourier transform of $S_{fat}(t_n)$ along the echo dimension. A_{norm} is a normalization factor, calculated from the net area of all peaks in the fat spectrum. This choice of normalization, together with the negligible T_1 weighting of the signal, ensures that

W and F in equation [1] represent the relative proton densities of water and fat in the tissue (14).

As suggested by the form of equation [1], the fitting procedure was implemented in the time domain. Data for each voxel were automatically truncated where the signal fell below twice the noise level. Calculations were performed in Matlab (Mathworks, Natick, Massachusetts) using the trust-region-reflective algorithm with the constraints $W \geq 0$, $F \geq 0$, and $R_2^* \geq 0$.

Analysis of R_2^* changes

To obtain summary measures for each subject, the marrow was manually segmented from cortical bone and surrounding tissue in both proximal femora. Structures containing trabeculae were analyzed separately from the diaphysis (femoral shaft), since the presence of trabeculae is known to shorten T_2^* (11). The structures containing trabeculae comprised the femoral head and neck, greater and lesser trochanters, and intertrochanteric region. For simplicity we will refer to them collectively as the hip.

The R_2^* response to ferumoxytol, denoted ΔR_2^*, was evaluated by subtracting baseline values from results at 3 days post-injection. To determine local R_2^* response, the 3-day images were coregistered to the baseline images using a 3D rigid-body transformation. ΔR_2^* could thus be calculated for each voxel. To determine the dependence of ferumoxytol uptake on marrow cellularity, we evaluated the correlation between ΔR_2^* and local water content as quantified by the proton density water fraction (PDWF)

$$\mathrm{PDWF}=\frac{W}{W+F}, \quad [3]$$

where W and F are determined from the numerical model in equation [1]. The PDWF thus defined may be considered an intrinsic property of the tissue by virtue of the fact that the model accounts for the spectral complexity of fat and the signal has negligible T_1 weighting (14).

Since the imaging slab was not thick enough to encompass the entire hip, ΔR_2^* could be calculated only for those voxels that lay within the intersection of the imaging volumes at the baseline and 3-day time points. Similarly, the FOV was not large enough to include the entire length of the femoral shaft. To ensure consistency among data sets, analysis was performed over the proximal 18 cm of the diaphysis.

To quantify iron elimination from bone marrow over the following five months, mean R_2^* values in the diaphysis were evaluated at each time point. Structures containing trabeculae were not included because the imaging slab did not cover exactly the same volume of the hip at each time point and regional variations in trabecular density would have introduced a confounding effect on mean R_2^* values.

Statistical analysis

Correlations were calculated using the Pearson linear correlation coefficient and comparisons were performed using the Student's *t*-test. Statistical significance was set at $P < 0.05$.

Results

No adverse reactions to ferumoxytol occurred. All participants completed the study and satisfactory image quality was obtained in all exams. The reference fat signal used for the fitting procedure was obtained from subcutaneous adipose tissue near the center of the FOV in a 57 year old woman with body mass index of 34.6 kg/m^2. The magnitude of the signal as a function of echo time is shown in Figure 1a, while the corresponding spectrum as a function of frequency shift is displayed in Figure 1b. Note the non-exponential decay of the signal (Figure 1a), which results from interference among the multiple spectral peaks (Figure 1b). The FWHM of the principal (methylene) peak was 7.4 Hz, corresponding to a relaxation time of $T_2^{*(\mathrm{fat})}=43\mathrm{ms}$, or, equivalently, a relaxation rate of $R_2^{*(\mathrm{fat})}=23\mathrm{s}^{-1}$.

Figure 2 shows spectra from red marrow in the proximal right diaphysis of a 41 year old man, both at baseline and 3 days after ferumoxytol administration. The baseline spectrum (Figure 2a) resembles the reference fat spectrum (Figure 1b) with the addition of a water peak at 0 Hz frequency shift. The presence of both lipid and water peaks reflects the mixture of adipocytes and hematopoietic elements contained in red marrow. Three days after ferumoxytol administration (Figure 2b), all the peaks are broadened, signifying a shortening of T_2^* (increase in R_2^*) for both lipid and water components.

Figure 3 displays the corresponding images and R_2^* maps from the same subject as Figure 2. The images on the left are reconstructed from the first echo of the MGRE acquisition, which had an echo time (TE) of 1.83 ms. At this TE value, the phase of the water signal is almost opposite that of the principal lipid component. Red marrow, which contains a mixture of adipocytes and hematopoietic elements, thus appears darker than yellow marrow, which consists mainly of fat. Comparison of the baseline gradient echo image (Figure 3a) with the corresponding R_2^* map (Figure 3b) shows that R_2^* differs little between red and yellow marrow at baseline. However, R_2^* is noticeably higher in the hip than the diaphysis due to the presence of trabeculae. Three days after ferumoxytol administration, R_2^* increases dramatically in red marrow but not in yellow marrow (Figure 3d). Visual inspection of the 3-day results reveals a close resemblance between the enhancement pattern on the R_2^* map (Figure 3d) and the anatomic distribution of red marrow on the gradient echo image (Figure 3c).

The graphs on the right of Figure 3 show the R_2^* response as a function of PDWF for this subject, both in the hip (Figure 3e) and the diaphysis (Figure 3f). Each point corresponds to a different voxel, whose location is mapped between the baseline and 3-day image sets by means of a 3D rigid-body transformation. Despite considerable scatter, high correlations are observed between ΔR_2^* and water content, confirming that ferumoxytol uptake is greater in red marrow than yellow marrow.

Similar results were obtained in the other five study participants. At baseline, R_2^* was marginally higher in red marrow than yellow marrow in all subjects, both in the diaphysis and the hip. The hip exhibited substantially higher R_2^* than the diaphysis, even after controlling for differences in water content. This suggests that the presence of trabeculae has a much greater effect than marrow cellularity on baseline R_2^* values.

In response to ferumoxytol, all subjects exhibited large R_2^* increases in red marrow, and lower average R_2^* changes in yellow marrow. In one participant (subject 4), the R_2^* response in red marrow was so great that T_2^* became too short to quantify at the 3-day time point using our 1.83 ms echo spacing. This person was the heaviest in the cohort, weighing 100 kg, and thus received the largest net dose of ferumoxytol (see Table 1). Due to the difficulty in obtaining accurate ΔR_2^* values in this individual, he was excluded from the quantitative analysis of ferumoxytol uptake and elimination. Over the remaining subjects, positive correlations were observed between ΔR_2^* and PDWF. The correlations were significantly higher in the hip (r = 0.77 ± 0.08) than the diaphysis (r = 0.29 ± 0.26), *P* = 0.016. Inspection of the R_2^* maps in cases of poor correlation revealed that the response to ferumoxytol was not limited exclusively to regions of red marrow, but also occurred in certain areas with high fat content.

Figure 4 shows an example in a 22 year old man. In the post-contrast R_2^* map (Figure 4d), note the focal area of strong R_2^* enhancement at mid-shaft in the left femur (arrow), in a region that appears, from its high intensity on the gradient echo image (Figure 4c), to be predominantly fat. Inspection of the fat and water maps in these voxels confirmed that the tissue composition was indeed primarily fat with very low water content. The R_2^* enhancement in the distal femora of this subject is also disproportionately high relative to local water content. In the hip, by contrast, the R_2^* enhancement pattern closely matches the anatomic distribution of red marrow. The plots of R_2^* response versus PDWF reflect these observations. In the hip (Figure 4e), the voxels fall into two distinct clusters, one with high water content, corresponding to red marrow and demonstrating a large R_2^* increase, and the other with low water content, representing yellow marrow and showing minimal R_2^* change. In the femoral shaft (Figure 4f), some voxels with low water content exhibit a disproportionately large R_2^* response, resulting in a weak correlation between ΔR_2^* and PDWF.

Figure 5 shows the R_2^* time course over the entire five-month period of the study for all subjects in whom uptake data were available. The points represent the mean of R_2^* over all voxels in the proximal 18cm of both femoral diaphyses without regard to their water content. The mean R_2^* responses at 3 days show considerable variation among study participants, with an average and standard deviation of $\Delta R_2^*{=}57 \pm 44\mathrm{s}^{-1}$. However, when normalized to mean PDWF (see Table 1), the individual responses were significantly correlated with the net dose of ferumoxytol in units of [mg Fe] (*r* = 0.88, *P* = 0.046). Data from follow-up scans reveal that, relative to peak values, R_2^* had recovered by 77 ± 7 % (mean ± standard deviation) at 1 month, 91 ± 7 % at 3 months, and 98 ± 5 % at 5 months.

Discussion

To our knowledge, this is the first human study of ferumoxytol uptake in bone marrow. While marrow imaging with other (U)SPIO agents has been the subject of several earlier investigations (2, 5–7, 15), ferumoxytol offers certain advantages over previously-used particles. First, it is the only agent to be widely approved for human use. Second, ferumoxytol can be injected as a rapid bolus, unlike ferumoxides (Feridex/Endorem) and ferumoxtran-10 (Combidex/Sinerem), which must each be administered as a slow infusion. Third, evidence suggests that ferumoxytol exhibits relatively high uptake in bone marrow compared to other agents; its small particle size ensures a longer plasma half-life and greater extravasation than the larger SPIO agents such as ferumoxides (2, 5, 15) and ferucarbotran (Resovist/Cliavist) (7). Furthermore, ferumoxytol has been found to elicit a larger MR response than ferumoxtran-10 at delayed time points in rats (10), although it is unclear whether the difference was due to greater uptake or slower metabolism.

Like other USPIO agents, ferumoxytol dramatically shortens T_1, T_2 and T_2^* values in solution. Following uptake by macrophages, however, the particles are compartmentalized within intracellular lysosomes. Aggregation restricts their interaction with surrounding water protons, reducing their T_1 shortening efficacy and allowing T_2 and T_2^* effects to predominate (16–17). We chose to measure T_2^* and to image after an interval equal to five times the reported plasma half-life of the agent in order to maximize the sensitivity to macrophage uptake and limit nonspecific intravascular and interstitial concentrations. Use of a multiple gradient echo sequence enabled quantitative measurement of the response to ferumoxytol as well as local fat/water ratio, providing a means to determine the relationship between ferumoxytol uptake and marrow cellularity.

We observed large R_2^* increases in red marrow at 3 days following ferumoxytol administration, but lower average responses in yellow marrow. Voxel-wise plots of R_2^* response versus water content demonstrated considerable scatter (see examples in Figures 3 and 4). This was likely due to imperfect coregistration between baseline and 3-day data sets and to the effect of image noise on measurements of R_2^* and fat/water ratio. However, all subjects exhibited high correlations between R_2^* response and water content in the hip, suggesting greater uptake of ferumoxytol by hematopoietic marrow than by fatty marrow. The correlations were lower in the femoral shaft, due to disproportionate uptake by some regions with high fat content.

Our observation of high uptake in red marrow is consistent with results of earlier USPIO-enhanced imaging studies and with existing knowledge about the hematopoietic microenvironment. Signal loss in hematopoietic marrow on T_2^*-weighted images at delayed time points has previously been reported in rodents following administration of ferumoxytol (10) and ferumoxtran-10 (9). In the latter study, histological examination with Perls' Prussian blue revealed intense iron-positive staining of hematopoietic bone marrow and no extracellular iron deposits. Experiments in rodents using carbon particles of similar diameter have shown that extravasation occurs through diaphragmatic fenestrations in the endothelium of the bone marrow sinusoids (18). Once in the bone marrow interstitium, the particles are rapidly taken up by parenchymal macrophages (19). Sequestration of carbon particles by intrasinusoidal macrophages (19) and sinusoidal endothelial cells (20) has also been demonstrated. Studies of aspirated human marrow confirm that macrophages, reticular cells and sinusoidal endothelial cells all play a phagocytic role in humans (21).

The uptake distribution of ferumoxytol particles among different cell types in bone marrow has not, to our knowledge, been reported. However, the above evidence suggests that macrophages, reticular cells and sinusoidal endothelial cells may all potentially be involved. These cells constitute the principal elements of the marrow stroma, which provides physical support for hematopoietic cells as well as growth factors and cell surface proteins that influence proliferation and differentiation. The sinusoidal endothelium regulates cellular traffic between the bone marrow and the vascular lumen, removing senescent cells from the blood and releasing new cells back into the circulation (22). It is also believed to provide a specialized microenvironment, termed the ‘vascular niche’, for maintenance and self-renewal of hematopoietic stem cells (22–23). Macrophages are present near the abluminal surface of the sinusoids (21) and at the center of erythroblastic islands, where they play the role of ‘nurse cells’, regulating erythropoiesis through cell-cell interactions and secretion of cytokines (24). Macrophages and reticular cells also process cellular debris, including senescent erythrocytes, abnormal erythroblasts and nuclei extruded by erythroblasts at the terminal phase of differentiation (21, 24). As such, they serve an important function in the recycling and delivery of iron, which is required for erythropoiesis (25). Collectively, these stromal cells form the basis of the hematopoietic microenvironment, without which hematopoiesis cannot occur (26). Their phagocytic capacity and abundance within hematopoietic marrow underlie the avid uptake of USPIO particles.

With age, the amount of hematopoietic marrow declines, as it is replaced by fatty marrow. Adipose conversion occurs in a gradual and predictable manner, starting at the extremities and progressing towards the axial skeleton (27–28). Within the long bones, such as the femora, it begins in the epiphyses and apophyses, and then continues in the diaphysis, advancing on two fronts towards the distal metaphysis, and, more slowly, towards the proximal metaphysis (27–29). Reconversion of fatty marrow back to hematopoietic marrow occurs in response to increased demand for hematopoiesis and proceeds in the reverse order. Our imaging findings are consistent with this pattern. In all subjects, the femoral head and greater trochanter displayed low water content, characteristic of yellow marrow. The femoral neck and intertrochanteric region exhibited areas with intermediate water content, indicative of red marrow, which contains both adipocytes and hematopoietic elements. In the diaphyses, the water content showed large regional variations but tended to decrease with distance distally.

Yellow marrow has a sparse vascular supply and consists predominantly of adipocytes (30). The relative paucity of hematopoietic elements is consistent with our observation of lower average uptake of ferumoxytol in yellow marrow. However, we also found that certain regions of the diaphysis exhibited substantial R_2^* response despite having high fat content. To our knowledge, the only similar result in the literature is a report of signal changes in yellow marrow following USPIO administration in juvenile rabbits (4). This result may not be entirely comparable with ours, however, since the marrow physiology of juvenile rabbits differs substantially from that of adult humans. Furthermore, the rabbits were imaged only one hour after USPIO injection, which may not have been sufficient for the agent to have completely cleared the blood pool. In our study, post-contrast imaging was performed after a delay equal to five times the reported plasma half-life of the agent, so it is reasonable to assume that the R_2^* responses reflect intracellular uptake of the particles rather than nonspecific intravascular concentration.

Our observation of substantial R_2^* increases in certain regions with high fat content suggests uptake of ferumoxytol by residual stromal cells in otherwise fatty marrow. The hypothesis that residual stroma may persist in predominantly fatty marrow has some support in the literature. It is known, for example, that adipose conversion is a reversible process, involving accumulation of lipids by adventitial reticular cells that surround the abluminal surface of the marrow sinusoids (22). The resulting enlargement of the cells constricts the lumen of the sinusoids, thereby limiting blood flow without compromising the integrity of the endothelial wall (22). Preservation of the sinusoids is essential for the reestablishment of hematopoiesis and for the maintenance of hematopoietic stem cells (22). It has also been shown that proliferation of myelosupportive stroma precedes the appearance of hematopoietic cells in transplanted marrow (31). These findings suggest that residual sinusoidal structures, comprising endothelium, adventitial reticular cells and macrophages, may persist in a quiescent state following adipose conversion, and proliferate in response to increased demand for hematopoiesis. We envision this process as occurring on a dynamic basis as the marrow adapts to fluctuations in demand. Since the cells of the marrow stroma are phagocytic, their continued presence may explain the anomalous R_2^* increases that we observed in certain regions with high fat content. The fact that these disproportionate R_2^* responses occurred in the diaphysis but not the hip may be related to the anatomic sequence of marrow conversion. To test these hypotheses would require histological studies, which fall outside the scope of the present work. Our data concerning iron elimination from bone marrow are consistent with those obtained by Vande Berg *et al.* following injection of the SPIO agent ferumoxides in two healthy human subjects (5). Our results showed 77% recovery of R_2^* by 1 month and 98% recovery by 5 months. Vande Berg *et al.* measured T_2 rather than T_2^*, but reported a progressive increase in bulk T_2 values over 3 weeks and almost complete recovery to pre-contrast values within 6 months. The length of time taken for iron elimination from the marrow, and from other organs such as the liver (32), is an important consideration in the use of (U)SPIO agents for diagnostic purposes.

In keeping with convention, we chose to calculate the injected dose on the basis of body weight. However, our results showed widely differing responses among the study participants. In our heaviest subject, who received the largest net dose, R_2^* dephasing was too rapid to quantify at day 3 using the 1.83 ms echo spacing. Over the remaining five subjects, ΔR_2^* in the diaphysis was significantly correlated with net dose after correction for fat/water ratio. These findings suggest that, if the objective is to obtain a similar response in hematopoietic marrow across all subjects, it may not be optimal to calculate dose according to body weight. Instead, it may be preferable to fix the net dose, independent of body weight, or to adjust the dose in accordance with body surface area or some other surrogate of total metabolic rate (33).

We performed post-contrast imaging three days after ferumoxytol administration to allow the agent time to clear from the blood pool and thereby ensure that the R_2^* responses would reflect intracellular uptake. The need for two visits, however, makes the protocol less convenient for clinical applications. Previous studies of other USPIO agents have involved delays as short as 20 minutes (2, 6). While this holds obvious practical advantages, it may complicate interpretation of the images (34).

By performing T_2^* mapping, we were able to obtain quantitative results, maximize sensitivity to ferumoxytol uptake and estimate fat content simultaneously. A potential drawback of T_2^* mapping, however, is the confounding effect of trabecular density on T_2^* values (11). We circumvented this problem by subtracting baseline R_2^* values from post-contrast measurements. However, this required separate acquisitions and coregistration of the resulting data sets. Quantification may be useful in detecting diffuse disease, such as multiple myeloma. However, if quantification is not necessary, it may be simpler to use fat-suppressed T_2-weighted imaging.

This preliminary study was aimed at quantifying and understanding ferumoxytol uptake in normal marrow, and we did not investigate the effect of marrow pathology. Other limitations included the small number of subjects and the fact that one participant had to be excluded from the quantitative analysis of uptake and elimination because his 3-day post-contrast T_2^* values were too short to evaluate.

The image analysis also involved a number of approximations that should be recognized. In using a reference fat signal obtained from subcutaneous fat in a single subject, we implicitly assumed that the fat spectrum of marrow is similar to that of subcutaneous fat and comparable across different subjects. While the first assumption is relatively well justified (35), there are known to be minor differences in lipid composition among individuals, specifically regarding the length of the carbon chains and the fraction of fatty acids that are mono- or polyunsaturated. These differences, which arise in part from diet (36–37), affect the relative amplitudes of the spectral peaks (35, 38). Our use of the same fat reference for all subjects was dictated by practical considerations and a desire for consistency, and we believe that it had minimal impact on the final results.

Another approximation made in the spectral fitting was the use of a single R_2^* value for water and lipid signals within the same voxel. This was based on the premise that magnetic field heterogeneity caused by USPIO particles or endogenous susceptibility variations affects both water and fat signals equally. This assumption is supported by the similarity in width between the water and lipid peaks in our red marrow spectra (see Figure 2). Furthermore, it was necessary from a practical perspective since incorporation of separate T_2^* values for water and lipids into the numerical model would have made the fitting procedure unstable.

One final comment is warranted regarding the length of the echo train. Our choice of a very long echo train permitted calculation of a spectrum for each voxel, and was advantageous for this preliminary study since it provided a means to check the validity of the assumptions outlined above. However, in future studies it should be sufficient to use a much shorter echo train, with duration of the order of the longest T_2^* value among the tissues of interest.

In conclusion, we have shown that ferumoxytol produces large R_2^* increases in normal hematopoietic marrow at delayed imaging, and lower average responses in fatty marrow. This is characteristic of macrophage-specific uptake, and may be useful in distinguishing normal or hypercellular marrow from neoplasms, infection and inflammation. To evaluate the clinical utility of ferumoxytol for diagnostic marrow imaging, further studies will be needed in specific patient populations.

Acknowledgments

Grant support: NIH HL092439

References

1. Weissleder R, Elizondo G, Wittenberg J, Rabito CA, Bengele HH, Josephson L. Ultrasmall superparamagnetic iron oxide: characterization of a new class of contrast agents for MR imaging. Radiology. 1990; 175:489–493. [PubMed: 2326474]
2. Daldrup-Link HE, Rummeny EJ, Ihssen B, Kienast J, Link TM. Iron-oxide-enhanced MR imaging of bone marrow in patients with non-Hodgkin's lymphoma: differentiation between tumor infiltration and hypercellular bone marrow. Eur Radiol. 2002; 12:1557–1566. [PubMed: 12042968]
3. Daldrup-Link HE, Henning T, Link TM. MR imaging of therapy-induced changes of bone marrow. Eur Radiol. 2007; 17:743–761. [PubMed: 17021706]
4. Seneterre E, Weissleder R, Jaramillo D, et al. Bone marrow: ultrasmall superparamagnetic iron oxide for MR imaging. Radiology. 1991; 179:529–533. [PubMed: 2014305]
5. Vande Berg BC, Lecouvet FE, Kanku JP, et al. Ferumoxides-enhanced quantitative magnetic resonance imaging of the normal and abnormal bone marrow: preliminary assessment. J Magn Reson Imaging. 1999; 9:322–328. [PubMed: 10077032]
6. Metz S, Lohr S, Settles M, et al. Ferumoxtran-10-enhanced MR imaging of the bone marrow before and after conditioning therapy in patients with non-Hodgkin lymphomas. Eur Radiol. 2006; 16:598–607. [PubMed: 16284770]
7. Fukuda Y, Ando K, Ishikura R, et al. Superparamagnetic iron oxide (SPIO) MRI contrast agent for bone marrow imaging: differentiating bone metastasis and osteomyelitis. Magn Reson Med Sci. 2006; 5:191–196. [PubMed: 17332709]
8. Bierry G, Jehl F, Boehm N, Robert P, Dietemann JL, Kremer S. Macrophage imaging by USPIO-enhanced MR for the differentiation of infectious osteomyelitis and aseptic vertebral inflammation. Eur Radiol. 2009; 19:1604–1611. [PubMed: 19198846]
9. Bierry G, Jehl F, Boehm N, et al. Macrophage activity in infected areas of an experimental vertebral osteomyelitis model: USPIO-enhanced MR imaging--feasibility study. Radiology. 2008; 248:114–123. [PubMed: 18458246]
10. Simon GH, Raatschen HJ, Wendland MF, et al. Ultrasmall superparamagnetic iron-oxide-enhanced MR imaging of normal bone marrow in rodents: original research original research. Acad Radiol. 2005; 12:1190–1197. [PubMed: 16099684]
11. Machann J, Stefan N, Schick F. (1)H MR spectroscopy of skeletal muscle, liver and bone marrow. Eur J Radiol. 2008; 67:275–284. [PubMed: 18406092]
12. Chandarana H, Lim RP, Jensen JH, et al. Hepatic iron deposition in patients with liver disease: preliminary experience with breath-hold multiecho T2*-weighted sequence. AJR Am J Roentgenol. 2009; 193:1261–1267. [PubMed: 19843739]
13. Pai AB, Nielsen JC, Kausz A, Miller P, Owen JS. Plasma pharmacokinetics of two consecutive doses of ferumoxytol in healthy subjects. Clin Pharmacol Ther. 2010; 88:237–242. [PubMed: 20592725]

14. Reeder SB, Cruite I, Hamilton G, Sirlin CB. Quantitative assessment of liver fat with magnetic resonance imaging and spectroscopy. J Magn Reson Imaging. 2011; 34:729–749. [PubMed: 21928307]
15. Hundt W, Petsch R, Helmberger T, Reiser M. Effect of superparamagnetic iron oxide on bone marrow. Eur Radiol. 2000; 10:1495–1500. [PubMed: 10997443]
16. Simon GH, Bauer J, Saborovski O, et al. T1 and T2 relaxivity of intracellular and extracellular USPIO at 1.5T and 3T clinical MR scanning. Eur Radiol. 2006; 16:738–745. [PubMed: 16308692]
17. Muller RN, Gillis P, Moiny F, Roch A. Transverse relaxivity of particulate MRI contrast media: from theories to experiments. Magn Reson Med. 1991; 22:178–182. discussion 195–176. [PubMed: 1812343]
18. Bankston PW, De Bruyn PP. The permeability to carbon of the sinusoidal lining cells of the embryonic rat liver and rat bone marrow. Am J Anat. 1974; 141:281–285. [PubMed: 4416404]
19. Hudson G, Yoffey JM. Reticulo-Endothelial Cells in the Bone Marrow of the Guinea-Pig. J Anat. 1963; 97:409–416. [PubMed: 14047359]
20. De Bruyn PP, Michelson S, Becker RP. Endocytosis, transfer tubules, and lysosomal activity in myeloid sinusoidal endothelium. J Ultrastruct Res. 1975; 53:133–151. [PubMed: 172648]
21. Wickramasinghe SN. Observations on the ultrastructure of sinusoids and reticular cells in human bone marrow. Clin Lab Haematol. 1991; 13:263–278. [PubMed: 1794229]
22. Bianco P. Bone and the hematopoietic niche: a tale of two stem cells. Blood. 2011; 117:5281–5288. [PubMed: 21406722]
23. Nagasawa T, Omatsu Y, Sugiyama T. Control of hematopoietic stem cells by the bone marrow stromal niche: the role of reticular cells. Trends Immunol. 2011; 32:315–320. [PubMed: 21531624]
24. Chasis JA, Mohandas N. Erythroblastic islands: niches for erythropoiesis. Blood. 2008; 112:470–478. [PubMed: 18650462]
25. Leimberg MJ, Prus E, Konijn AM, Fibach E. Macrophages function as a ferritin iron source for cultured human erythroid precursors. J Cell Biochem. 2008; 103:1211–1218. [PubMed: 17902167]
26. Crocker PR, Gordon S. Isolation and characterization of resident stromal macrophages and hematopoietic cell clusters from mouse bone marrow. J Exp Med. 1985; 162:993–1014. [PubMed: 4031789]
27. Kung JW, Yablon CM, Eisenberg RL. Bone marrow signal alteration in the extremities. AJR Am J Roentgenol. 2011; 196:W492–W510. [PubMed: 21512037]
28. Laor T, Jaramillo D. MR imaging insights into skeletal maturation: what is normal? Radiology. 2009; 250:28–38. [PubMed: 19092089]
29. Waitches G, Zawin JK, Poznanski AK. Sequence and rate of bone marrow conversion in the femora of children as seen on MR imaging: are accepted standards accurate? AJR Am J Roentgenol. 1994; 162:1399–1406. [PubMed: 8192007]
30. Dwek JR, Shapiro F, Laor T, Barnewolt CE, Jaramillo D. Normal gadolinium-enhanced MR images of the developing appendicular skeleton: Part 2. Epiphyseal and metaphyseal marrow. AJR Am J Roentgenol. 1997; 169:191–196. [PubMed: 9207523]
31. Tavassoli M, Crosby WH. Bone marrow histogenesis: a comparison of fatty and red marrow. Science. 1970; 169:291–293. [PubMed: 4247471]
32. Storey P, Lim RP, Chandarana H, et al. MRI assessment of hepatic iron clearance rates after USPIO administration in healthy adults. Invest Radiol. 2012; 47:717–724. [PubMed: 23070094]
33. Gibson S, Numa A. The importance of metabolic rate and the folly of body surface area calculations. Anaesthesia. 2003; 58:50–55. [PubMed: 12523324]
34. Daldrup-Link HE, Mohanty A, Cuenod C, Pichler B, Link T. New perspectives on bone marrow contrast agents and molecular imaging. Semin Musculoskelet Radiol. 2009; 13:145–156. [PubMed: 19455477]
35. Ren J, Dimitrov I, Sherry AD, Malloy CR. Composition of adipose tissue and marrow fat in humans by 1H NMR at 7 Tesla. J Lipid Res. 2008; 49:2055–2062. [PubMed: 18509197]

36. Field CJ, Angel A, Clandinin MT. Relationship of diet to the fatty acid composition of human adipose tissue structural and stored lipids. Am J Clin Nutr. 1985; 42:1206–1220. [PubMed: 4072956]

37. van Staveren WA, Deurenberg P, Katan MB, Burema J, de Groot LC, Hoffmans MD. Validity of the fatty acid composition of subcutaneous fat tissue microbiopsies as an estimate of the long-term average fatty acid composition of the diet of separate individuals. Am J Epidemiol. 1986; 123:455–463. [PubMed: 3946391]

38. Berglund J, Ahlstrom H, Kullberg J. Model-based mapping of fat unsaturation and chain length by chemical shift imaging--phantom validation and in vivo feasibility. Magn Reson Med. 2012; 68:1815–1827. [PubMed: 22334300]

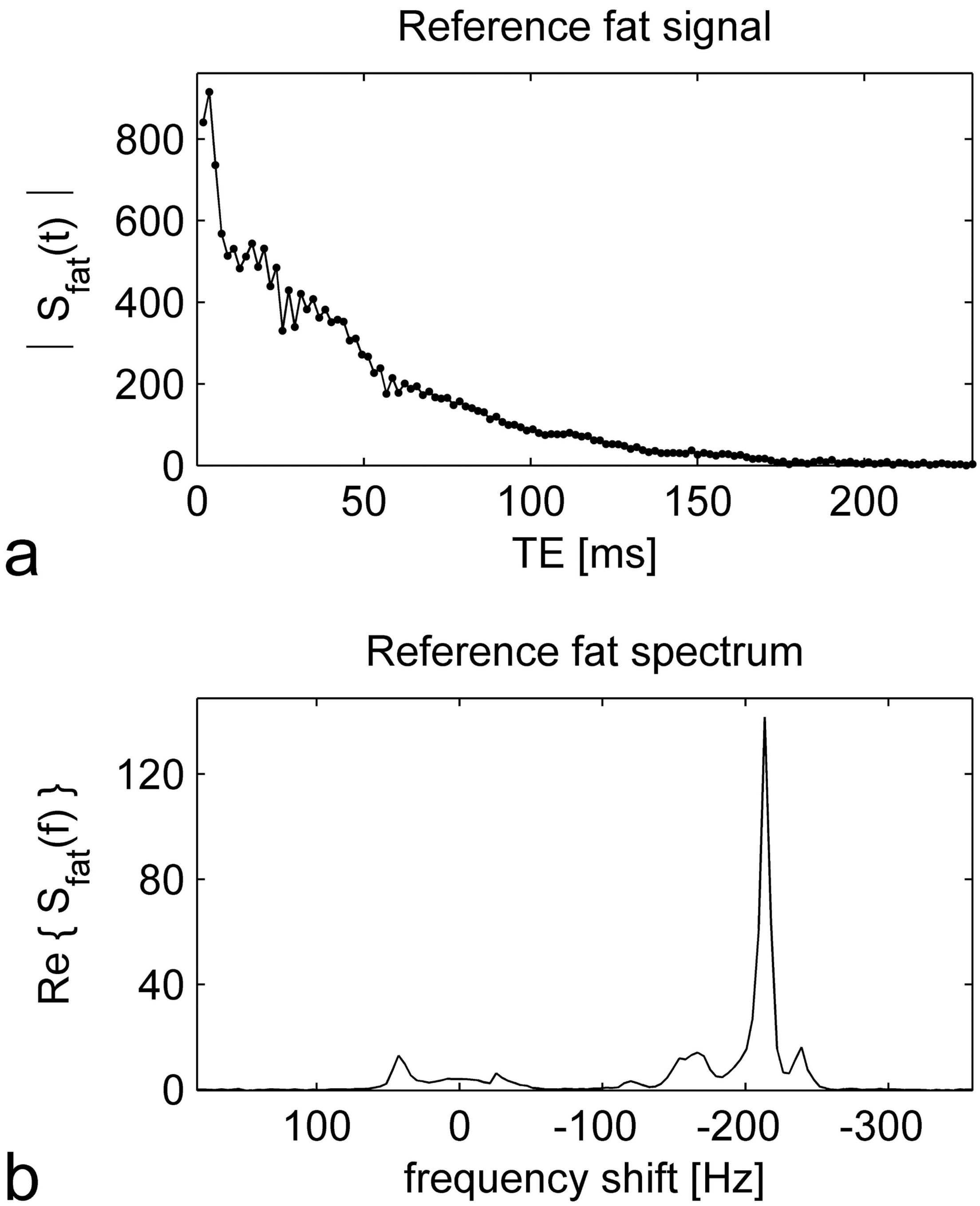

Figure 1.

The reference fat signal measured in subcutaneous adipose tissue of a 57 year old woman and used in the fitting procedure to generate maps of fat, water and R_2^*. The upper graph (a) shows the magnitude of the signal as a function of echo time (TE), acquired using the multiple gradient echo (MGRE) sequence. The lower graph (b) displays the corresponding spectrum as a function of frequency shift from the water resonance. The spectrum was calculated from the complex-valued MGRE signal by performing a Fourier transform over the echo dimension. Data from several adjacent voxels were combined to improve the signal to noise ratio (SNR), but no apodization was applied. The vertical axes of both graphs are plotted in arbitrary units.

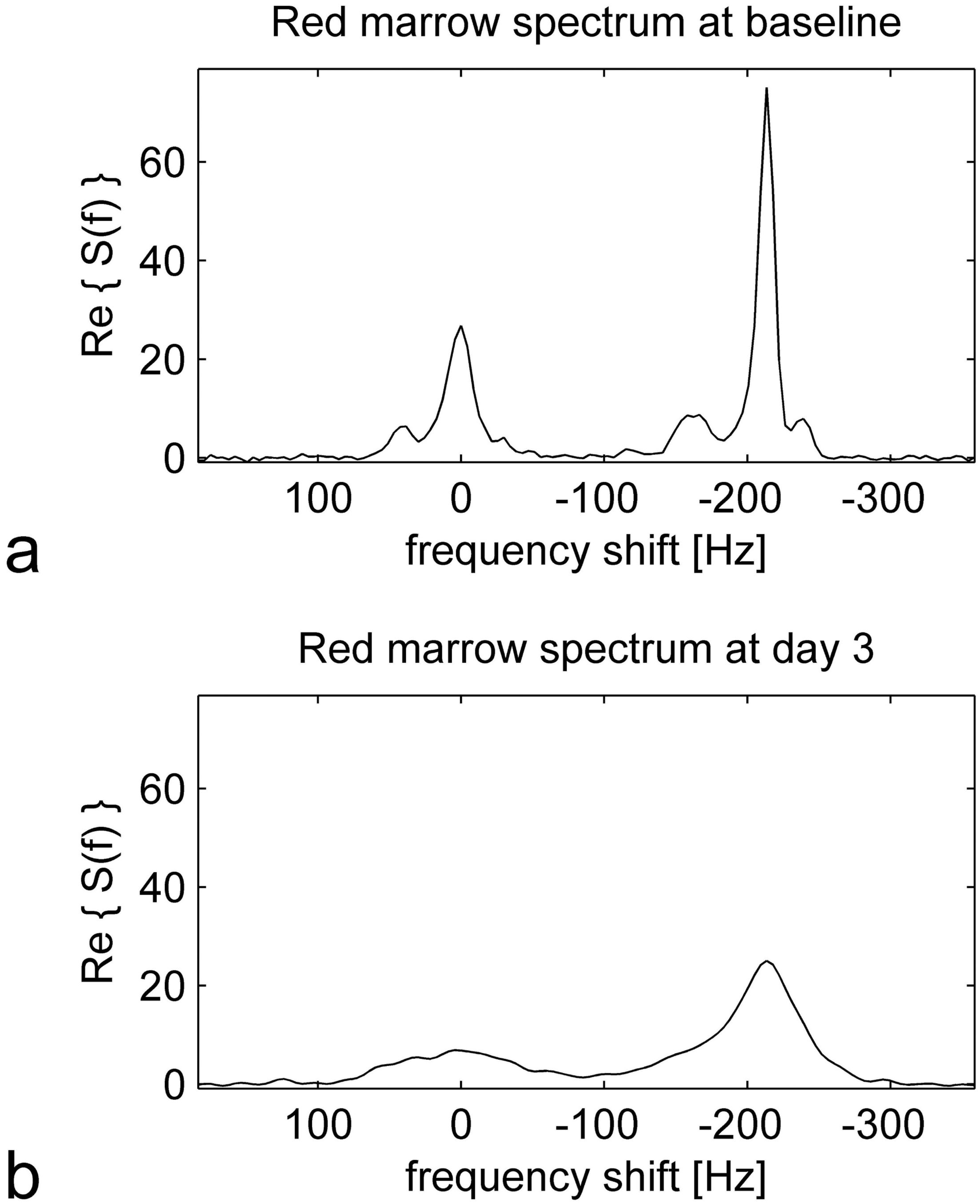

Figure 2.

Spectra from red marrow in the proximal right diaphysis of a 41 year old man at baseline (a) and 3 days after ferumoxytol administration (b). As in Figure 1, the spectra were obtained from the MGRE signal by performing a Fourier transform over the echo dimension, and data from several adjacent voxels were combined to improve SNR. Note that the baseline spectrum (a) resembles the reference fat spectrum (Figure 1b) with the addition of a peak at 0 Hz frequency shift corresponding to water. Both the lipid and water peaks are broadened in response to ferumoxytol administration (b), reflecting a shortening of T_2^* (increase in R_2^*).

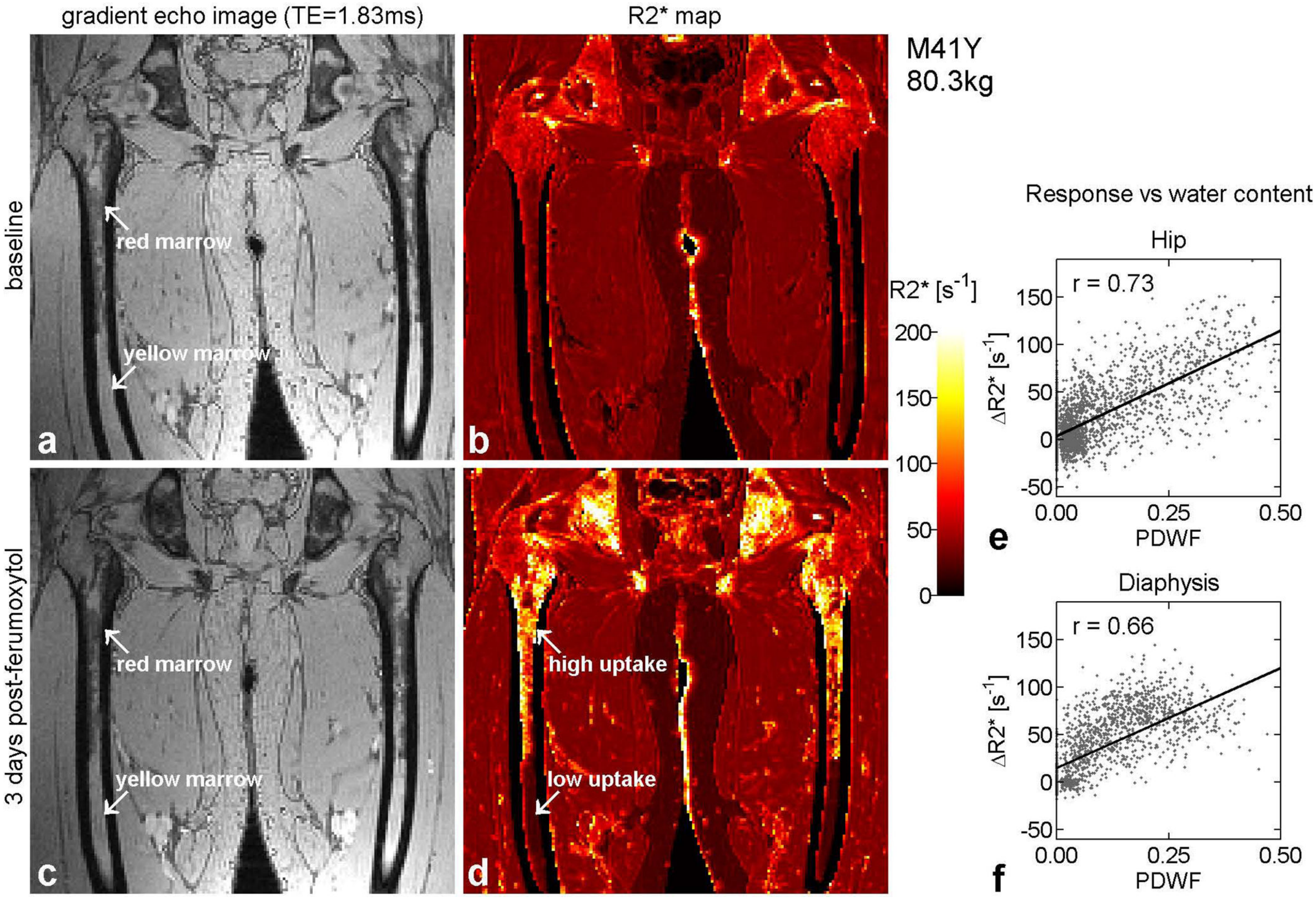

Figure 3.

Gradient echo images and R_2^* maps from the same subject as in Figure 2, illustrating regional variations in the response to ferumoxytol. Panels (a) and (b) show results from baseline, while panels (c) and (d) are from day 3. On the left are raw images reconstructed from the first echo of the MGRE acquisition, with TE = 1.83 ms. Due to the relative phases of fat and water at this echo time, red marrow appears relatively dark while yellow marrow is brighter. Panels (b) and (d) show the corresponding R_2^* maps, which are displayed using the adjacent color scale. Regions such as background and cortical bone, where the signal was too low to fit, are displayed in black. Between baseline and day 3, R_2^* increases dramatically in red marrow but remains low in yellow marrow (arrows). Detailed inspection shows that the enhancement pattern on the post-contrast R_2^* map (d) closely matches the anatomic distribution of red marrow on the gradient echo image (c). The slight geometric distortion, responsible for the ‘bow-legged’ appearance of the femora in panels (a) – (d), is due to the fact that the images were reconstructed offline, without access to information concerning the nonlinearity of the imaging gradients. The graphs on the right depict the R_2^* response to ferumoxytol in each voxel as a function of proton density water fraction (PDWF), both in the hip (e) and the diaphysis (f).

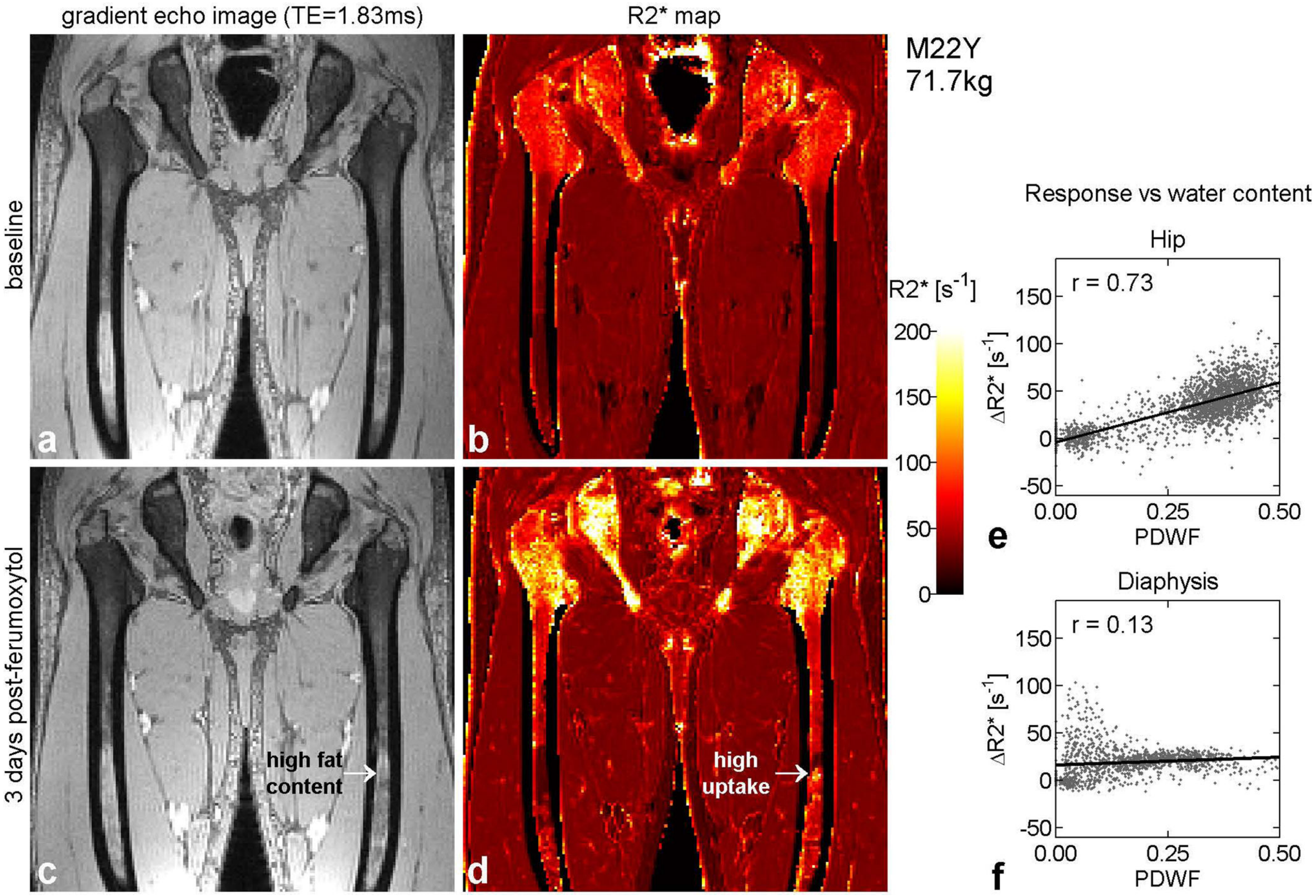

Figure 4.

Results from a 22 year old man, displayed in the same format as Figure 3. In the hip, the pattern of R_2^* enhancement (d), closely matches the distribution of red marrow (c), as in Figure 3. This correlation is reflected in graph (e), which shows two well-separated clusters of points, one with high water content, corresponding to red marrow and demonstrating a large R_2^* increase, and the other with low water content, representing yellow marrow and showing minimal R_2^* change. In the diaphysis, however, the correlation between PDWF and R_2^* response is weaker, as shown in graph (f). This can be traced to the relatively large R_2^* responses that occur in certain regions with high fat content. For example, a focal area of high uptake is observed at mid-shaft in the left femur (arrow) despite the high fat content in that region. In addition, the distal diaphyses of both femurs exhibit disproportionately large R_2^* responses relative to local water content.

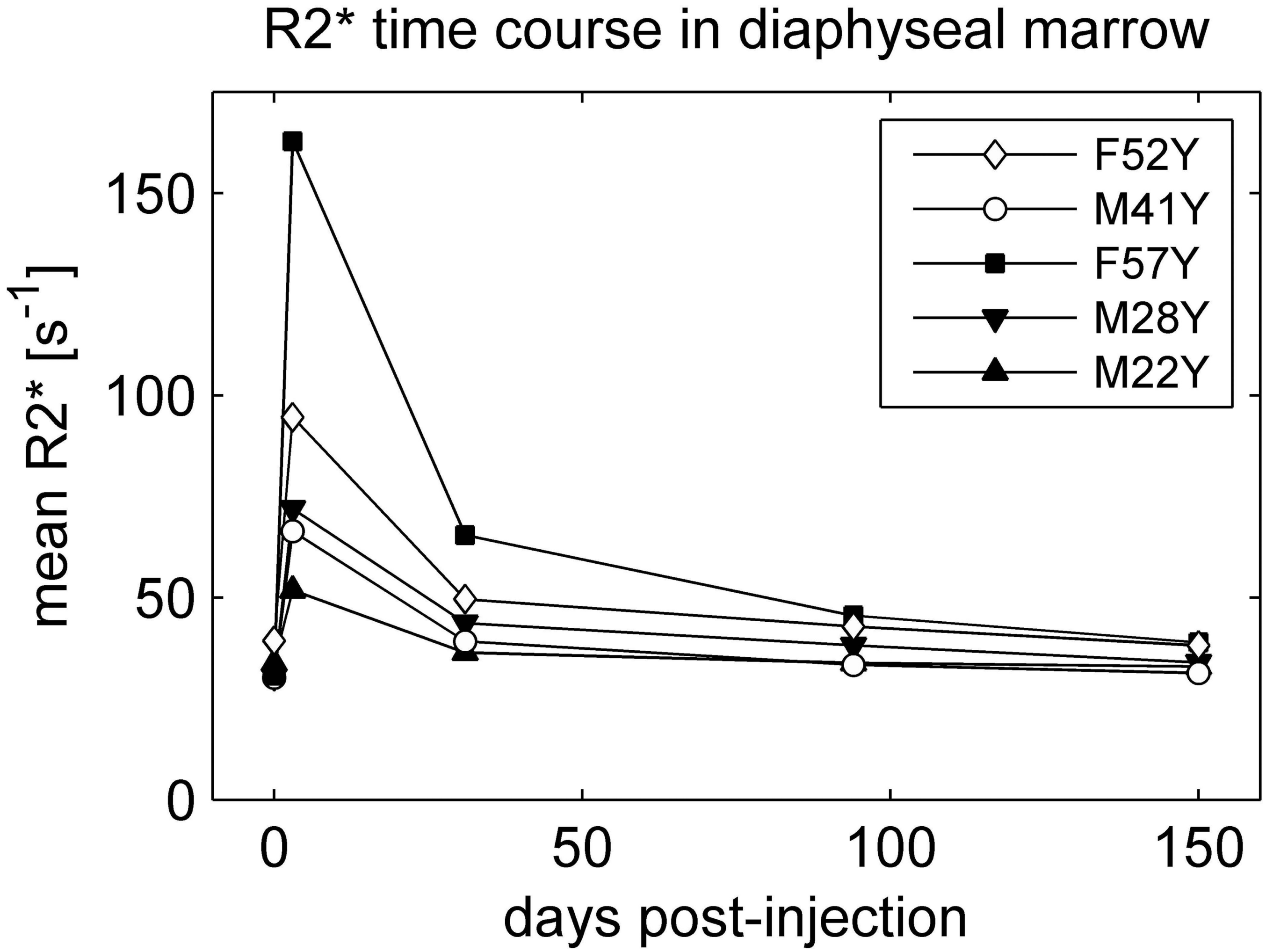

Figure 5.

Mean R_2^* in diaphyseal marrow as a function of time over the entire 5-month period of the study. Baseline values are plotted at day zero. R_2^* is averaged over all marrow voxels in the proximal 18cm of the diaphyses regardless of their water content. PDWF for each subject is provided in Table 1.

Table 1

Demographic information and mean water content in diaphyseal marrow

subject	sex/age	weight/height	BMI[§]	Net dose of ferumoxytol[‡]	PDWF in diaphyseal marrow[†]
1	F / 52	63.5 kg/153 cm	27.1 kg/m^2	318 mg Fe	0.23
2	M / 41	80.3 kg/160 cm	31.4 kg/m^2	401 mg Fe	0.11
3	F / 57	97.5 kg/168 cm	34.6 kg/m^2	488 mg Fe	0.08
4[*]	M / 25	100.2 kg/176 cm	32.5 kg/m^2	501 mg Fe	0.04
5	M / 28	79.4 kg/178 cm	25.1 kg/m^2	397 mg Fe	0.12
6	M / 22	71.7 kg/179 cm	22.5 kg/m^2	358 mg Fe	0.17

[§] Body mass index, defined as BMI = weight [kg] / (height [m])^2

[‡] Dose is proportional to body weight, i.e. 5 mg Fe/kg

[†] Proton density water fraction (PDWF) calculated according to equation [3] and averaged over the proximal 18 cm of the femoral shaft.

[*] Excluded from the quantitative analysis of ferumoxytol uptake and elimination, since T_2^* in red marrow was too short to quantify at day 3.